

# RSC Advances



This is an *Accepted Manuscript*, which has been through the Royal Society of Chemistry peer review process and has been accepted for publication.

*Accepted Manuscripts* are published online shortly after acceptance, before technical editing, formatting and proof reading. Using this free service, authors can make their results available to the community, in citable form, before we publish the edited article. This *Accepted Manuscript* will be replaced by the edited, formatted and paginated article as soon as this is available.

You can find more information about *Accepted Manuscripts* in the [Information for Authors](#).

Please note that technical editing may introduce minor changes to the text and/or graphics, which may alter content. The journal's standard [Terms & Conditions](#) and the [Ethical guidelines](#) still apply. In no event shall the Royal Society of Chemistry be held responsible for any errors or omissions in this *Accepted Manuscript* or any consequences arising from the use of any information it contains.

**Effect of reaction temperature on properties of carbon nanodots and their visible-light photocatalytic degradation of tetracycline**

**Qiong Wu,<sup>a</sup> Wei Li,<sup>a</sup> Peng Wu,<sup>a</sup> Jian Li,<sup>a</sup> Shouxin Liu,<sup>a\*</sup> Chunde Jin<sup>b</sup> and Xianxu Zhan<sup>c</sup>**

*<sup>a</sup>College of Materials Science and Engineering, Northeast Forestry University, Harbin 150040, China*

*\*Tel/ Fax: 86-451-82191204*

*E-mail address: liushouxin@126.com (S.X. Liu)*

*<sup>b</sup>Key Laboratory of Wood Science and Technology, Zhejiang Province, Hangzhou 310000, China*

*<sup>c</sup>Dehua TB New Decoration Co., Ltd, Huzhou 313200, China*

## Abstract

Water-soluble carbon nanodots (CND<sub>t</sub>) with diverse sizes, crystal structures, surface properties, and characteristic fluorescence spectra were synthesized by the hydrothermal carbonization of larch at different temperatures. The effects of reaction temperature on the diameter distribution, structural components, and fluorescence properties of the CND<sub>t</sub> were investigated systematically. The synthesized CND<sub>t</sub> were found to be monodispersed spherical polymer nanodots with a low degree of aromatization and abundant oxygen-containing groups on their surface. Increasing the reaction temperature decreased the average size of the nanodots from 20.35 to 6.48 nm, while their quantum yield increased from 13% to 18%. Broader and weaker UV characteristic peaks were detected when the reaction temperature was increased from 200 to 260 °C. All the CND<sub>t</sub> samples exhibited excitation and emission-independent properties, and obvious blue shift of the excitation and emission peaks occurred at higher reaction temperatures owing to the smaller size and different surface properties obtained. The CND<sub>t</sub> were used as a photosensitizer in a CND/TiO<sub>2</sub> system to effectively degrade tetracycline hydrochloride (TCH) under visible-light irradiation. The obvious blue shift exhibited by the smaller CND<sub>t</sub> allowed the light to be fully used by the TiO<sub>2</sub>, resulting in nearly 100% TCH degradation for CND<sub>260</sub>/TiO<sub>2</sub>.

*Keywords:* Water-soluble carbon nanodot; Visible-light photocatalytic; Hydrothermal carbonization; Larch; Reaction temperature.

## 1. Introduction

Antibiotics are used extensively worldwide in medical treatment and agriculture but are often poorly absorbed by humans and animals; 50% to 80% of all antibiotics drain out and enter the aquatic environment. These residues may induce soil toxicity, development of antibiotic-resistant pathogens, and other problems that may threaten human health [1-2]. For example, tetracyclines are the second most common antibiotics in both production and usage, and have been successfully used for treating various infectious diseases. However, there is still a lack of effective, complete, and systematic technologies for the removal of pollutants like tetracyclines. Compared with other methods such as adsorption and microbial degradation, photocatalytic degradation is a simple and

effective way of removing such macromolecular organic compounds in aqueous systems [3-4]. Photocatalysts can degrade macromolecules into non-toxic small molecules, inhibiting their toxic properties and restricting their transport in water thoroughly. Traditional semiconductors such as  $\text{TiO}_2$  and  $\text{SiO}_2$  are widely used for the photocatalytic removal of environmental pollution because they are good oxidants with high photocatalytic activity, chemical stability, and low toxicity. However, they can only effectively use a narrow spectral range of UV irradiation, which comprises 5% of incident sunlight.

The preparation and applications of quantum dots have attracted much attention because their quantum effects can give them unique properties. When particles are nanoscale, the size limit domain can give rise to size, quantum confinement, macroscopic quantum tunneling, and surface effects, resulting in chemical and physical properties different from those of macroscopic materials. Quantum dots have been widely used in the fields of bio-imaging, photocatalysis, medicine, and functional materials [5-8]. The emerging carbon nanodots successfully overcome the drawbacks of traditional semiconductor and metal quantum dots such as poor water-solubility, high toxicity, and incompatibility with biological environments, opening up new directions and broadening the scope in which quantum dots may be used. Carbon nanodots are a new kind of nanoscale particles consisting of carbon existing in the form of a conjugated system of  $\text{SP}^2$  hybridized and unsaturated  $\text{SP}^3$  hybridized carbon atoms, which creates obvious responses to light, electricity and magnetism [9-10]. Therefore, the search for a simple and environmentally friendly method of preparing carbon nanodots has become a hot topic.

The northeast of China is rich in larch resources, and a huge amount of sawdust waste is produced and discarded every year. The exploitation of such waste plays a significant role in the development of renewable energy sources [11-12]. Hydrothermal carbonization has been proved to be an effective way to convert biomass into useful functional carbon materials. Through this process, biomass can be hydrolyzed to generate various value-added polymer precursors from which carbon materials with controllable shapes and sizes can be obtained [13-14]. Carbon nanodots with ordered crystal lattices and frequency up-conversion properties have been successfully prepared via hydrothermal carbonization of biomass [15]. Our groups have previously synthesized water-soluble carbon nanodots with substantial fluorescence via

hydrothermal carbonization of pentosan extracted from pulp refining, which exhibited good photocatalytic properties under visible light [16].

Here, we report the synthesis of water-soluble carbon nanodots with diverse sizes, crystal structures, and optical properties, using larch as the carbon source. The particle size, quantum yield, and characteristic fluorescent peaks of the nanodots were controlled by adjusting the reaction temperature. The resulting  $CND_t$  were systematically investigated as a photosensitizer in a  $TiO_2$ -based photocatalytic system for the degradation of tetracycline hydrochloride.

## 2. Materials and Methods

### 2.1 Hydrothermal carbonization of larch to produce $CND_t$

In a typical experiment, larch biomass (1.5 g) was dispersed in distilled water (40 mL) and ultrasonically agitated for 15 min. The suspension was added to a stainless steel autoclave of 55 mL in volume. The autoclave was placed in a furnace at 200 °C, 220 °C, 240 °C, and 260 °C for 12 h, and then allowed to cool to room temperature. The resulting brown suspension was collected and subjected to centrifugation at 12000 rpm for 20 min. The light yellow supernatant containing the  $CND_t$  was subjected to dialysis (1000 Da molecular weight cutoff) for about 72 h before further characterization.

### 2.2 Preparation of the $CND/TiO_2$ system

$CND/TiO_2$  composites were synthesized using a sol-gel method [17]. Tetrabutyl titanate (0.5 mL) was dissolved in ethanol (20 mL) to form aqueous solution A, while water (9 mL) and aqueous ammonia (5 mL, 28%) were mixed to form aqueous solution B. Solution B was added to A in a dropwise manner with continual stirring and the mixture was left to age for 12 h. The resulting precipitate was collected by centrifugation, dried at 80 °C for 6 h, and then calcined at 500 °C for 1 h to yield  $TiO_2$ . The obtained  $TiO_2$  (0.1 g) was added to the  $CND_t$  solution (5 mL) with stirring over 10 min, followed by drying before further use.

### 2.3 Characterization

Transmission electron microscopy (TEM) images of the  $\text{CND}_t$  samples were obtained on a JEOL 2011 (FEI, Holland) operated at 200 kV. FT-IR spectra were recorded on a Fourier transform infrared (FT-IR) instrument (Perkin Elmer TV1900, Waltham, MA, USA) from 400–4000  $\text{cm}^{-1}$  at a resolution of 4  $\text{cm}^{-1}$ . X-ray photoelectron spectra were recorded on a Physical Electronics PHI 5400 spectrometer (Physical Electronics, USA) using Al-K $\alpha$  radiation ( $h\nu = 1486.6$  eV). Binding energies were referenced to the C $_{1s}$  line at 284.6 eV. Elemental analysis (C, H, O, and N) was carried out using an EA 3000 analyzer (EuroVector, Milan, Italy). UV-vis absorption spectra were obtained using a TU-1900 UV-vis spectrometer. Fluorescence spectroscopy was performed on a LS-55 fluorescence spectrophotometer (PerkinElmer, USA) equipped with a 120-W xenon lamp as the excitation source. The morphologies and sizes of the  $\text{CND}/\text{TiO}_2$  composites were observed using environmental scanning electron microscopy (SEM; Quanta 200, FEI, Hillsboro, OR, USA).

#### 2.4 Photocatalytic activity and quantum yield test

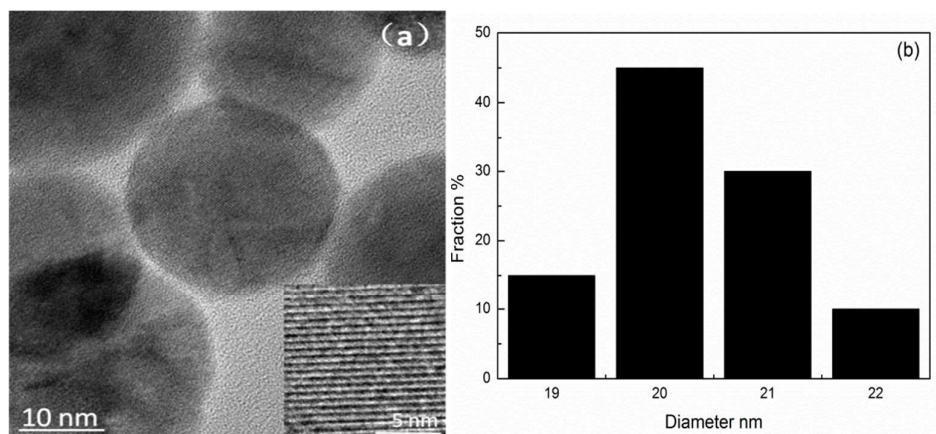
Photocatalytic activity tests were carried out in a cylindrical quartz photoreactor (275 mL) using TCH as the model compound and a 380-W Xe lamp (510 nm, Shanghai Hualun Lamp Factory, China) positioned inside the reactor as the light source. The photocatalyst powder (0.1 g) was added to 100 mL aqueous solution (50 mg/L). Before the photocatalytic degradation, the suspension was magnetically stirred in the dark for 20 min to establish TCH adsorption/desorption equilibrium. Aliquots of 5 mL were collected from the suspension and filtrated using a 0.22- $\mu\text{m}$  filter membrane. The concentration of TCH in the reaction solution after illumination was determined spectrophotometrically using a TU-1900 UV-vis spectrometer at 357 nm.

The fluorescence quantum yields of the  $\text{CND}_t$  were calculated using 5  $\mu\text{g mL}^{-1}$  Rhodamine B in ethanol as a standard (quantum yield 90%). The absorbance of Rhodamine B at 543 nm was less than 0.05. The calculation was performed according to the following equation:  $\Phi_u = \Phi_s (Y_u/Y_s)(A_s/A_u)$ , where u and s represent the  $\text{CND}_t$  and Rhodamine B, respectively,  $\Phi$  is the quantum yield, and Y is the integrated fluorescence area. A is the absorption at fluorescence excitation.

### 3. Results and Discussion

#### 3.1 Morphology of the $CND_t$

Changing the reaction temperature had a direct effect on the average diameter of the obtained  $CND_t$ , as shown in Table 1. TEM images and histograms of the size distribution of  $CND_{200}$  and  $CND_{260}$  are presented in Fig. 1, and clearly show that the  $CND_t$  were well dispersed spherical particles with different ordered lattice structures.  $CND_{200}$  exhibited a mean diameter of 20.35 nm (100 particles measured), and an obvious stripe-like hexagonal structure was detected on the surface. For  $CND_{260}$ , the average diameter was only 6.48 nm, and an ordered cubic structure was clearly seen. These results suggest that increased reaction temperature led to a decrease in size and change in lattice structure of the  $CND_t$ . As the hydrothermal process mainly involved dehydration, polymerization, aromatization and carbonization [18], various water-soluble organic products were also produced in the HTC process, including sugars and organic acids, maximum sugar and organic acids concentrations were obtained under low-temperature conditions but degraded considerably at higher temperatures [19], besides, higher reaction temperature favor carbonization [20], which means reaction was more completely at higher temperature with more condensed carbon structure, leading to the size of carbon dots decreased as temperature increased.



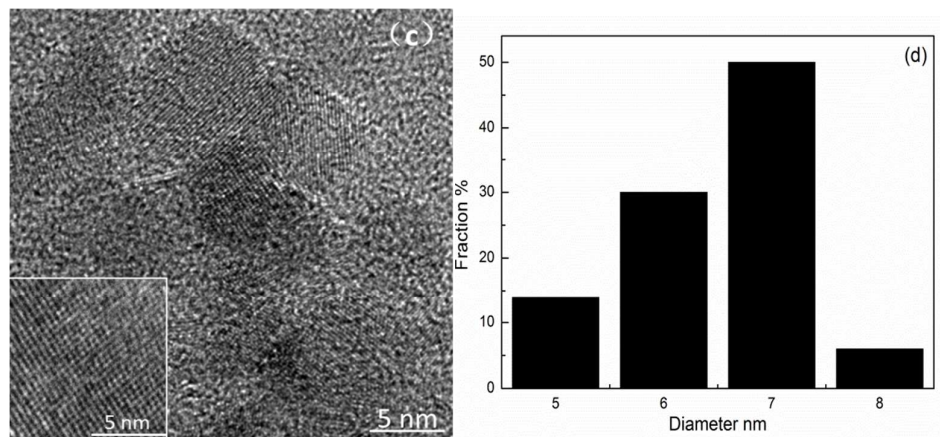


Fig. 1 TEM images and corresponding diameter distributions of CND<sub>200</sub> (a, c) and CND<sub>260</sub> (b, d).

### 3.2 Surface properties of the CND<sub>t</sub>

FT-IR analysis (Fig. 2 (a)) was used to reveal the functional groups on the surface of the raw material and CND<sub>t</sub> samples. Larch wood is predominantly composed of cellulose, hemicelluloses, and lignin, which have large amounts of oxygen-containing surface groups such as hydroxyls, carbonyls, and carboxyls. The FT-IR peaks observed for CND<sub>200</sub> were similar to those of the raw materials, while the CND<sub>220</sub>, CND<sub>240</sub> and CND<sub>260</sub> samples showed peaks with obvious changes, in accordance with previous studies showing that 200 °C is too low for the wood structure to be broken down completely.

The bands observed at 3300–3500 cm<sup>-1</sup> and 1028 cm<sup>-1</sup> were assigned to C-OH groups. Compared with those observed for the raw materials, the intensity of these peaks was much lower for the samples prepared at high temperature, because such groups are easily degraded to intermediate products during hydrothermal carbonization. The new peaks appearing at 1000–1460 cm<sup>-1</sup> corresponded to the C-O stretching vibration, confirming that hydroxyl, ester, and ether groups had been generated [21]. The new peaks at 1625 and 875–750 cm<sup>-1</sup> were attributed to the stretching vibration of C=C and the out-of-plane bending vibration of aromatic C-H, respectively, confirming the formation of a large amount of aromatic structure [22]. Finally, the adsorption band at 1700 cm<sup>-1</sup> corresponded to carboxylate groups. These results indicate that the structure of the

larch wood had been completely destroyed to form carbon material containing aromatic structures rich in surface functional groups including hydroxyls, esters, ethers, carbonyls, and carboxylic groups.

The elemental compositions (measured by XPS) of the surface of the raw materials and  $\text{CND}_t$  samples are summarized in Table 1. The samples mainly contained C, O, and N elements, with trace amounts of Na, Si, Ca, and S. When the reaction temperature was increased from 200 °C to 260 °C, the content of C on the surface declined from 77.3% to 72.4%, while the O content increased from 20.2% to 25.9%. This further confirmed that the  $\text{CND}_t$  were condensed carbon materials with a large amount of oxygen-containing groups. In detail, the ratio of O and C exhibited an obvious rising trend with reaction temperature, different from that observed for previously obtained solid products [20]. This was caused by the increased number of molecules available for polymerization, confirming that the structure of the  $\text{CND}_t$  samples may have been different from those of CSs. The present  $\text{CND}_t$  may have been polymer nanodots rich in oxygen-containing groups with a low degree of aromatization [23].

XPS was conducted to analyze the chemical composition of  $\text{CND}_{260}$ .  $\text{C}_{1s}$ ,  $\text{O}_{1s}$ ,  $\text{N}_{1s}$ , and Na peaks were observed, as shown in Fig. 2 (b). The XPS results indicated that these nanodots were mainly composed of C, O, and N, as well as a limited amount of Na element. The high C and O content confirmed that a condensed material with abundant oxygen-containing groups was produced at 260 °C. The  $\text{C}_{1s}$  spectrum was fit to four curves and attributed to aliphatic groups C-C (283.9 eV), C-N (285.2), C-O (286.1), and C=O/C=N (287.3) [18, 22, 24]. The  $\text{O}_{1s}$  spectrum exhibited three peaks at 533.4, 534.3, and 535.5 eV, which were attributed to O-C=O, C-OH/C-O-C groups, and chemically adsorbed oxygen, respectively [23]. These results indicate the presence of an aromatic structure and abundant oxygen-containing groups on the surface of  $\text{CND}_{260}$ .

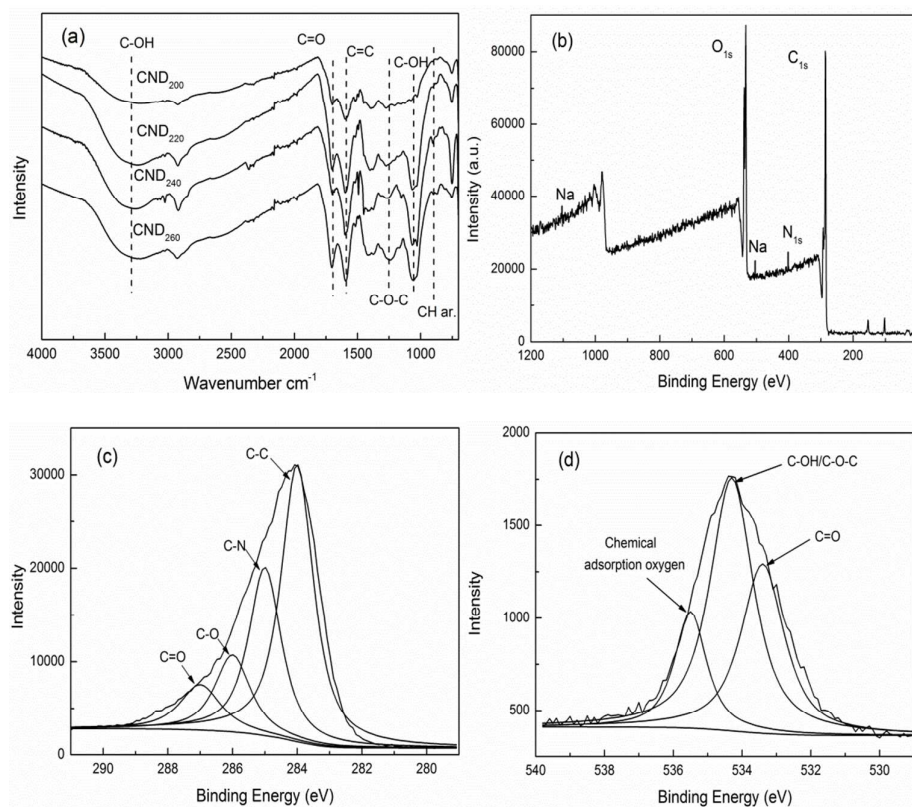


Fig. 2 FT-IR spectra (a) and XPS survey spectrum (b), high-resolution  $C_{1s}$  peaks and the fitting curves (c) and high-resolution  $O_{1s}$  peaks and fitting curves (d).

**Table 1 Average diameters and XPS analysis (wt %) of  $CND_t$**

Sample	Average diameter (nm)	C (wt %)	O (wt %)	N (wt %)	Others (wt %)	O/C(%)
$CND_{200}$	20.35	77.31	20.17	0.21	2.31	26.09
$CND_{220}$	16.4	78.35	19.80	0.16	1.69	25.22
$CND_{240}$	11.9	77.92	20.37	0.41	1.30	26.14
$CND_{260}$	6.48	72.38	25.85	0.27	1.50	35.71

### 3.3 Optical properties of the $CND_t$

UV-vis and PL spectra were measured to investigate the optical properties of the  $CND_t$  samples. All obtained samples were water-soluble and formed light yellow aqueous solutions. The UV-vis absorption spectra exhibited a high and obvious peak around 281 nm, as shown in Fig. 3. This can be attributed to complex electron transition on the surface, the  $\pi$  conjugated aromatic system, and the  $n-\pi^*$  transition of the carbonyl and other oxygen-containing groups [25-26]. It can be clearly seen that increased reaction temperatures led to the characteristic peak becoming broader and weaker, as the conjugate system is to reduce the total energy and increase the stability [27], the structure of the  $CND_t$  prepared at low temperature was incomplete with lower stability, hence causing the conjugate peak to be more obvious. This result is consistent with the FT-IR analysis.

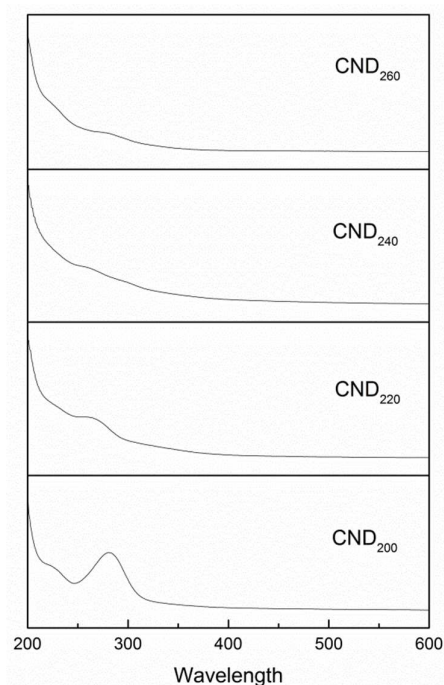


Fig. 3 UV-Vis absorption spectrum of  $CND_t$  samples.

The emission spectrum of  $CND_{200}$  at around 400–600 nm exhibited a peak at 440 nm upon

excitation at 350 nm. A corresponding peak centered at 350 nm in the excitation spectrum appeared at an emission wavelength of 440 nm. With increasing hydrothermal temperature, both the excitation and emission peaks exhibited blue shift to lower wavelength, as shown in Table 2. It is well known that the PL properties of a material can be attributed to energy-level transition, surface energy traps, and the radiative recombination of electrons and holes [28], as well as interactions between electrons and holes and the environment around them. Additionally, polycyclic aromatic compounds within the CNDs may have been responsible for their excellent PL properties [29].

Size is an important factor that affects the excitation and emission wavelengths, and can give a material special characteristics [30]. Furthermore, changes in structural and surface properties such as the degree of aromatization and amount of oxygen-containing groups can cause changes in the energy-level difference between the first excited state and ground states, leading to changes in the energy of absorbed and emitted photons, showing as obvious blue shift [31].

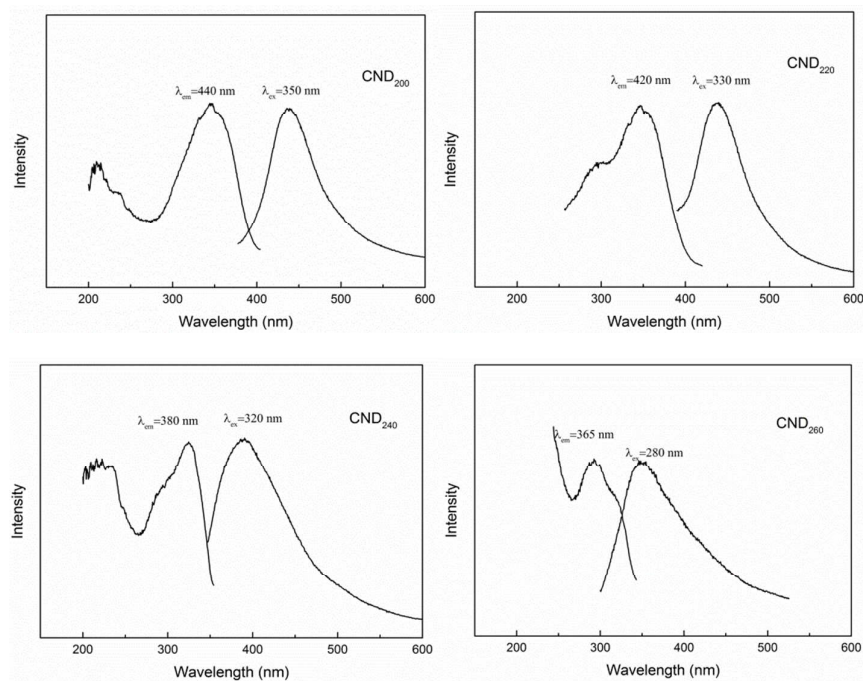


Fig. 4 PL emission and excitation spectra of CND<sub>t</sub> samples.

The PL spectra also indicated that the maximum emission and its intensity had a direct relationship with the excitation wavelength; this is a PL characteristic of C dots [32]. For CND<sub>200</sub>, upon changing the excitation wavelength from 260 to 420 nm, the emission peak red-shifted from 428 to 493 nm with a gradual decrease in intensity. Therefore, visible emission from CND<sub>200</sub> over the blue-to-red wavelength range was obtainable using the same sample under UV and visible excitation. For samples prepared at different temperatures, the excitation wavelength exhibited no obvious shift, while the main peak of the emission spectrum shifted from 440 nm to around 360 nm, in accordance with the analysis above.

Using Rhodamine B in ethanol as a standard, the quantum yield of CND<sub>200</sub> was calculated to be about 13.4%, higher than that of most reported CNDs [23,28]. The quantum yield increased obviously to 18.1% for CND<sub>260</sub>, confirming that increasing the reaction temperature caused an increase in quantum yield (as shown in Table 2).

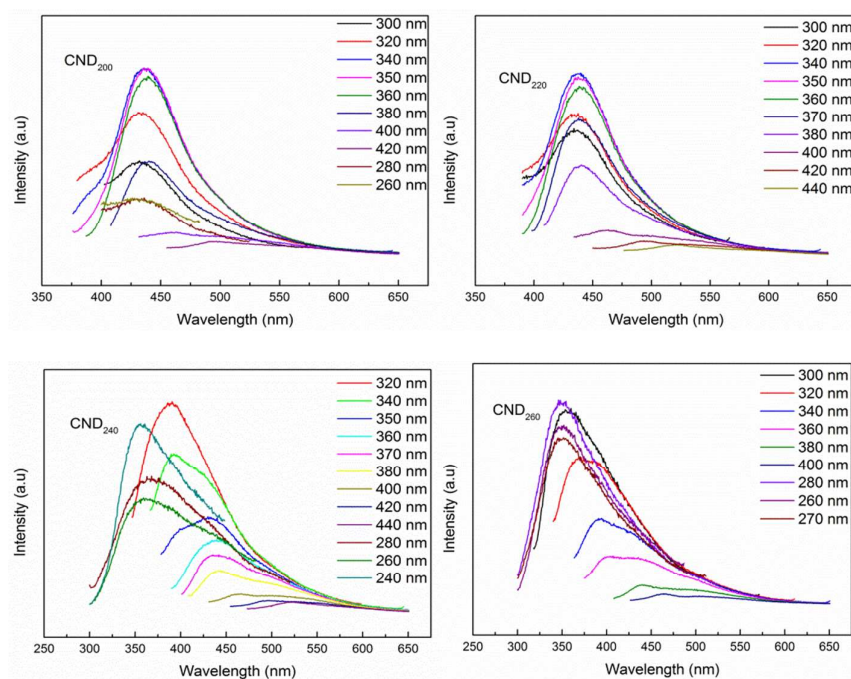


Fig. 5 Emission spectra of CND<sub>t</sub> at different excitation wavelengths.

### 3.4 pH sensitivity and chemical stability tests

Digital photos and emission spectra of CND<sub>220</sub> at different pH, adjusted using a sodium

bicarbonate and sodium carbonate buffer solution, are shown in Fig. 6. All prepared samples (CND<sub>200</sub>, CND<sub>220</sub>, CND<sub>240</sub>, and CND<sub>260</sub>) exhibited color ranging from light yellow to dark yellow as the pH was varied from 4.0 to 10.0. The intensity of the emission peak decreased with increasing pH without a change in wavelength, as previously reported [33]. The abundant oxygen-containing groups on the surface imparted acid properties to the CNDs, so at high pH values an increasing negative charge density accumulated on the surface. This influenced the  $\pi$ - $\pi^*$  and  $n$ - $\pi^*$  electronic transitions, leading to the observed color changes and fluorescence quenching.

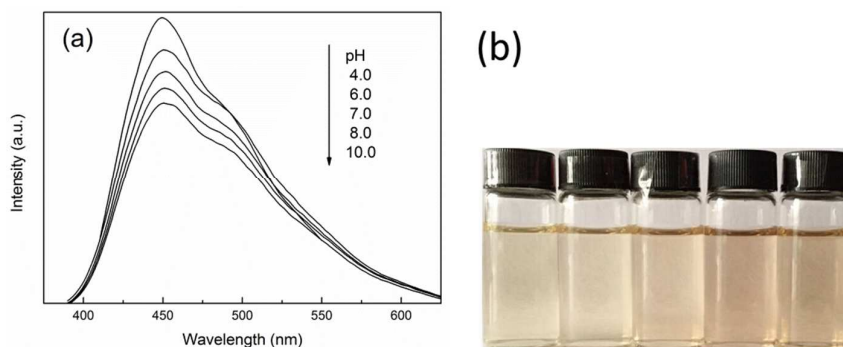


Fig. 6 PL spectra of CND<sub>220</sub> excited at 320 nm in solutions of different pH.

To investigate the chemical stability, FL quantum yields (QY) and optical absorption intensity (OAI) of CND<sub>t</sub> synthesized for six weeks were tested as shown in Table 2. They all exhibit good stability on both quantum yields (QY) and optical absorption intensity even samples lasted for six weeks. Both the QY and fluorescence intensity keep almost constant, confirming the chemical stability of obtained CND<sub>t</sub>.

**Table 2 Quantum yields and optical absorption intensity parameters of CND<sub>t</sub> synthesized for six weeks**

	QY(%)	QY <sub>a</sub> (%)	OAI(a.u.)	OAI <sub>a</sub> (a.u.)
CND <sub>200</sub>	13.4	13.0	673.5	642.1

CND <sub>220</sub>	14.9	14.5	685.2	650.9
CND <sub>240</sub>	16.6	16.1	692.9	658.3
CND <sub>260</sub>	18.1	17.2	693.4	662.1

*QY= Sample Quantum Yield*

*QY<sub>a</sub>= Quantum yield of samples synthesized for six weeks*

*OAI= Optical Absorption Intensity*

*OAI<sub>a</sub>= Optical Absorption Intensity of samples synthesized for six weeks*

*Optical Absorption Intensity was tested via irradiation by their respective characteristic excitation wavelength.*

The photochemical was tested by fluorescence Intensity Vs time of carbon nanodots under continuous UV irradiation (using UV lamp with power of 30 W, wavelength of 254 nm, light intensity of 107 uw/cm<sup>2</sup>), the results show that under constant UV illumination for 5 h, the Fluorescence Intensity remained constant, almost no bleaching was observed, suggesting the emission was quite stable.

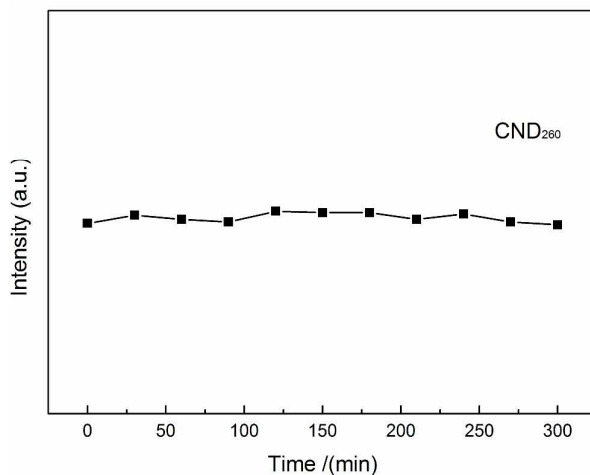


Fig. 7 Photochemical stability of CND<sub>260</sub> under continuous UV irradiation

The decay curve of synthesized  $CND_t$  were measured by HORIBA Fluoromax-4, from Fig.8 it can be clearly seen the decay curve of  $CND_{260}$  can be very well fitted to triple-exponential function, the lifetimes are  $\tau_1 = 8.34$ ,  $\tau_2 = 2.59$  and  $\tau_3 = 1.26$  ns, and the mean lifetime is calculated to be 5.48 ns, which is longer than previous reports [34]; based on the same calculation method, the life time was 3.23 ns, 4.32 ns, 5.06 ns and 5.48 ns for  $CND_{200}$ ,  $CND_{220}$ ,  $CND_{240}$ , and  $CND_{260}$  respectively.

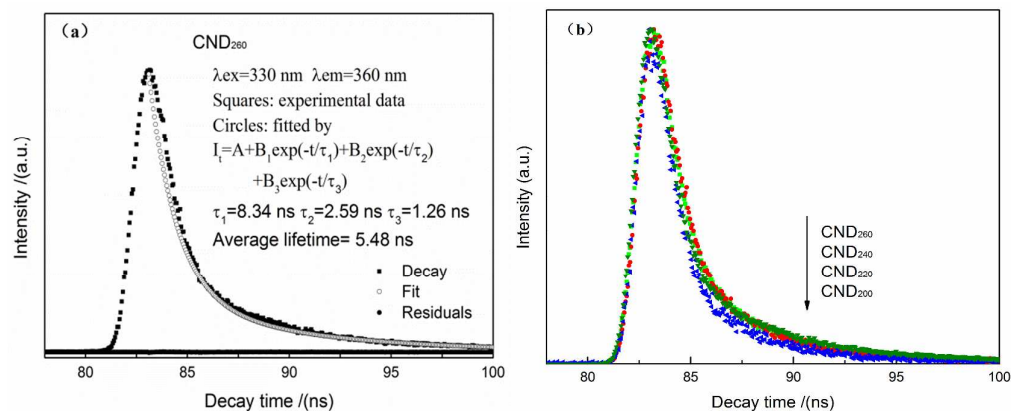


Fig. 8 Fluorescence decay curve and the fitting curve of  $CND_{260}$  (a) decay curve comparison of  $CND_t$

### 3.5 Photocatalytic activity of $CND/TiO_2$

The  $CND_t$  samples investigated here were rich in oxygen-containing groups and have been proved to be easily attached in a stable manner to the surface of  $TiO_2$  [35]. The  $CND$  were combined with  $TiO_2$  in a composite system, as shown in Fig. 9 (a) and (b). The corresponding HRTEM image shows that  $CND_{260}$  (lattice spacing 0.22 nm) were in close contact with the anatase  $TiO_2$  nanoparticles with the (101) crystal plane exposed (lattice spacing 0.35 nm), confirming that  $CND_t$  were successfully attached to the surface of the  $TiO_2$ .

The visible-light catalytic activities of the prepared  $CND_t/TiO_2$  composites were evaluated using the decomposition of tetracycline hydrochloride (TCH) under visible-light irradiation, as shown in Fig. 9 (c). Only 9.6% and 12.5% TCH reduction were obtained when pure  $CND_{200}$  and

TiO<sub>2</sub> were used as catalysts, respectively, and were mainly because of adsorption. Although the photocatalytic efficiency of P-25 was higher than pure CND<sub>200</sub> and TiO<sub>2</sub>, the value was still low of only 21%. The CND<sub>*t*</sub>/TiO<sub>2</sub> composites all gave efficient catalysis with high TCH degradation, indicating that interaction between the CNDs and TiO<sub>2</sub> occurred. The CND<sub>200</sub>/TiO<sub>2</sub> composite exhibited a good photocatalytic activity and gave around 89.7% TCH degradation. The saturated adsorption value was low under the dark condition, confirming that the observed decrease in TCH concentration mainly derived from photocatalytic degradation. The degradation efficiency reached 93.6%, 95.9% and 99.0% for CND<sub>220</sub>/TiO<sub>2</sub>, CND<sub>240</sub>/TiO<sub>2</sub> and CND<sub>260</sub>/TiO<sub>2</sub>, respectively, as shown in Table 3. Nearly 100% degradation of TCH was obtained for CND<sub>260</sub>/TiO<sub>2</sub>.

The proposed degradation mechanism is as follows (Fig. 9 (d)): the CND<sub>*t*</sub> with abundant oxygen-containing groups are sensitizer, when irradiation by visible light they can act as a photosensitizer and absorb photons. Photons with adequate energy can excite electrons in the HOMO, thus transferring them to the LUMO of the CND<sub>*t*</sub>. Free electrons as well energy can then be transferred to the conduction band of TiO<sub>2</sub> [36]. When the energy is equal or greater than the band-gap energy of TiO<sub>2</sub>, conduction band electrons (e<sup>-</sup>) and valence band holes (h<sup>+</sup>) are generated. In this system, photogenerated holes could either recombine with electrons, react with OH<sup>-</sup> or H<sub>2</sub>O, oxidizing them to highly oxidizing species such as OH• and O<sub>2</sub>•radicals, or oxidize the adsorbed TCH molecules [6]. Such highly oxidizing species were responsible for the decomposition of TCH by TiO<sub>2</sub>. Additionally, the photogenerated electrons could reduce adsorbed TCH or react with electron acceptors such as O<sub>2</sub> adsorbed on the TiO<sub>2</sub> surface or dissolved in water, reducing them to super-oxide radical anion O<sub>2</sub>•<sup>-</sup>, which can be transformed to OH• radicals by further reactions. In neutral conditions, reversible isomerization of asymmetric carbon atoms can occur, forming epimers of TCH. These epimers and their dehydration products are the main degradation products [34].

As discussed above, higher synthesis temperature led to changes in the size, structure, surface properties of the CND<sub>*t*</sub> as well the amount of oxygen-containing groups on their surface [21]. These changes can cause changes in the energy-level difference between the first excited state and ground states, leading to changes in the energy of absorbed and emitted photons, showing as obvious blue shift of emission and excitation spectra [30], CND<sub>260</sub> exhibited smallest size with

most abundant oxygen-containing groups, have strongest response to light irradiation, hence,  $\text{CND}_{260}/\text{TiO}_2$  exhibited the highest photocatalytic activity.

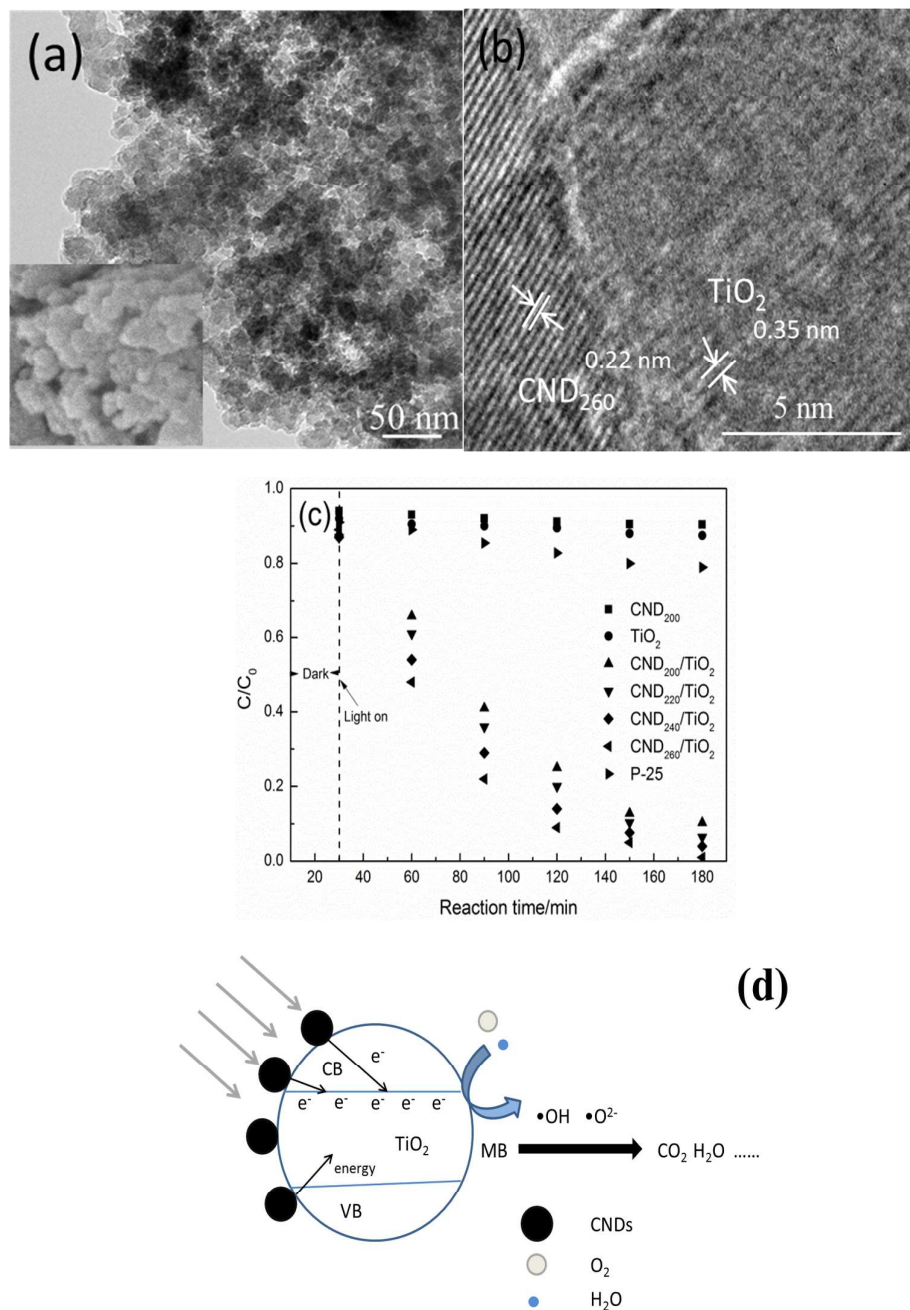


Fig. 9 (a) (b) SEM and corresponding high-resolution TEM images of  $\text{CND}/\text{TiO}_2$  composite, (c) TCH degradation percentage vs time curves and (d) catalytic mechanism for  $\text{CND}/\text{TiO}_2$  under visible-light irradiation.

**Table 3 Characteristic parameters of  $CND_t$** 

samples	Average Diameter (nm)	Quantum Yield (%)	Characteristics excitation wavelength (nm)	Characteristics emission wavelength (nm)	Photocatalytic degradation efficiency as photosensitizer (%)
$CND_{200}$	20.35	13.4	350	440	89.7
$CND_{220}$	16.4	14.9	330	420	93.6
$CND_{240}$	11.9	16.6	320	380	95.9
$CND_{260}$	6.48	18.1	280	365	99.0

#### 4. Conclusion

Water-soluble carbon nano dots ( $CND_t$ ) were synthesized via one-pot simple hydrothermal carbonization of lignocellulose-larch at different temperatures. The as-prepared  $CND_t$  were nanoscale spherical polymers with a low degree of aromatization and abundant oxygen-containing groups. They exhibited excellent photoluminescence (PL), excitation-dependence, and pH sensitivity, and their size, crystal structure, surface properties, and fluorescence characteristics could be varied by changing the reaction temperature from 200 °C to 260 °C. Increasing the reaction temperature decreased the average size and increased the fluorescence quantum yield of the  $CND_t$ , and was accompanied by variation in their ordered lattice structure from an obvious stripe-like hexagonal structure to a cubic structure. An obvious blue shift of the excitation and emission peaks was also observed, which arose from the differences in size and surface properties.

A  $CND/TiO_2$  system was found to be an effective photocatalyst;  $CND_t$  loaded on the surface of  $TiO_2$  acted as a photosensitizer. The spectral response of the composite system could hence be widened from the UV region to the visible-light region. Effective degradation of tetracycline hydrochloride (TCH) was achieved under visible-light irradiation.  $CND_t$  with smaller size, higher quantum yield and shorter excitation characteristic peak wavelength were found to be more

beneficial as a photosensitizer in the CND/TiO<sub>2</sub> system; nearly 100% TCH degradation was obtained for CND<sub>260</sub>/TiO<sub>2</sub>.

## Acknowledgements

This work was financially supported by grants from Special Fund for Forest Scientific Research in the Public Welfare (201504605), the Fundamental Research Funds of the Central Universities (2572014EB01), the National Natural Science Foundation of China (No. 31170545), and Zhejiang Key level 1 Discipline of Forestry Engineering (2014lygcz017).

## References

- [1] B. Halling-Sørensen, S. Nors-Nielsen, P. F. Lanzky, F. Ingerslev, H. C. Holten-Lutzhøft, S. E. Jørgensen, Occurrence, fate, and effects of pharmaceutical substances in the environment. A review, *Chemosphere*, 36 (1998) 357–393.
- [2] A. Pruden, R. Pei, H. Storteboom, K. H. Carlson, Antibiotic resistance genes as emerging contaminants: Studies in Northern Colorado, *Environmental Science & Technology*, 40 (2006) 7445-7450.
- [3] Y. B. Liu, X. J. Gan, B. X. Zhou, B. T. Xiong, J. H. Li, C. P. Dong, J. Bai, W. M. Cai, Photoelectrocatalytic degradation of tetracycline by highly effective TiO<sub>2</sub> nanopore arrays electrode. *Journal of Hazardous materials*, 171(2009) 678-683.
- [4] C. Zhao, Y. Zhou, D. J. de Ridder, J. Zhai, Y. M. Wei, H. P. Deng, Advantages of TiO<sub>2</sub>/5A composite for photocatalytic degradation of antibiotic oxytetracycline in aqueous solution: Comparison between TiO<sub>2</sub> and TiO<sub>2</sub>/5A composite system. *Chemical Engineering Journal*, 248 (2014) 280-289.
- [5] Q. H. Liang, W. J. Ma, Y. Shi, Z. Li, X. M. Yang, Easy synthesis of highly fluorescent carbon quantum dots from gelatin and their luminescent properties and applications, *Carbon*, 60, (2013) 421-428.

- [6] H. T. Li, X. D. He, Z. H. Kang, H. Huang, Y. Liu, J. L. Liu, S. Y. Lian, C. H. A. Tsang, X. B. Yang, S. T. Lee, Water-soluble fluorescent carbon quantum dots and photocatalyst design, *Angewandte Chemie-International Edition*, 49(2010) 4430-4434.
- [7] L. Cao, S. Sahu, P. Anilkumar, C. E. Bunker, J. Xu, K. A. S. Fernando, P. Wang, E. A. Gulians, K. N. Tackett, Y. P. Sun, Carbon nanoparticles as visible-light photocatalysts for efficient CO<sub>2</sub> conversion and beyond, *Journal of the American chemical society*, 133 (2011), 4754-4757.
- [8] Xing Zhang, Hai Ming, Ruihua Liu, Xiao Han, Zhenhui Kang, Yang Liu, yonglai Zhang, Highly sensitive humidity sensing properties of carbon quantum dots films, *Materials research bulletin*, 48(2013) 790-794.
- [9] X. H. Wang, K. G. Qu, B. L. Xu, J. S. Ren, X. G. Qu, Multicolor luminescent carbon nanoparticles: Synthesis, supramolecular assembly with porphyrin, intrinsic peroxidase-like catalytic activity and applications, *Nano Research*, 4(2011) 908-920.
- [10] J. H. Shen, Y. H. Zhu, X. L. Yang and C. Z. Li, Graphene quantum dots: emergent nanolights for bioimaging, sensors, catalysis and photovoltaic devices, *Chemical Communications*, 48(2012) 3686-3699.
- [11] L. Zhao, L. Z. Fan, M. Q. Zhou, H. Guan, S. Y. Qiao, M. Antonietti, M-M. Titirici, Nitrogen-containing hydrothermal carbons with superior performance in supercapacitors, *Advanced Materials*, 22(2010) 5202-5206.
- [12] L. P. Xiao, Z. J. Shi, F. Xu, R. C. Sun, Hydrothermal carbonization of lignocellulosic biomass, *Bioresource Technology*, 118 (2012) 619-623.
- [13] Q. Wu, W. Li, J. Tan, S.X. Liu, Flexible cage-like carbon spheres with ordered mesoporous structures prepared via a soft-template/hydrothermal process from carboxymethylcellulose, *RSC Advances*, 4(2014) 61518-61524.
- [14] G. B. Barin, I. F. Gimenez, L. P. Costa, A. G. Souza Filho, L. S. Barreto, Hollow carbon nanostructures obtained from hydrothermal carbonization of lignocellulose biomass, *journal of materials science*, 49(2014) 665-672.

- [15] X. D. He, H. T. Li, Y. Liu, H. Huang, Z. H. Kang, S-T. Lee, Water soluble carbon nanoparticles: hydrothermal synthesis and excellent photoluminescence properties, *Colloids and surfaces B: biointerfaces*, 87 (2011) 326-332.
- [16] Q. Wu, W. Li, Y. J. Wu, Z. H. Huang, S. X. Liu, Pentosan-derived water-soluble carbon nano dots with substantial fluorescence: properties and application as a photosensitizer. *Applied surface science*, 315(2014) 66-72.
- [17] Q. Wu, W. Li, T. Tan, Y. J. Wu, S. X. Liu, Hydrothermal carbonization of carboxymethylcellulose: one-pot preparation of conductive carbon microspheres and water-soluble fluorescent carbon nanodots, *Chemical engineering journal*, 266 (2015) 112-120.
- [18] M. Sevilla, A. B. Fuertes, The production of carbon materials by hydrothermal carbonization of cellulose, *Carbon* 47 (2009) 2281-2289.
- [19] S. K. Hoekman, A. Broch, C. Robbins, B. Zielinska, L. Felix, Hydrothermal carbonization (HTC) of selected woody and herbaceous biomass feedstocks. *Biomass Conversion and Biorefinery*, 3 (2013) 113-126.
- [20] M. Li, W. Li, S.X. Liu, Control of the morphology and chemical properties of carbon spheres prepared from glucose by a hydrothermal method, *Journal of materials research*, 27 (2012) 1117-1123.
- [21] X. M. Sun, Y. D. Li, Colloidal carbon spheres and their core/shell structures with noble-metal nanoparticles, *Angewandte Chemie-International Edition*, 43(2004) 597-601.
- [22] S. X. Liu, J. Sun, Z. H. Huang, Carbon spheres/activated carbon composite materials with high Cr(VI) adsorption capacity prepared by a hydrothermal method, *Journal of Hazardous Materials*, 173 (2010) 377-383.
- [23] S. Liu, J. Q. Tian, L. Wang, Y. W. Zhang, X. Y. Qin, Y. L. Luo, A. M. Asiri, A. O. Al-youbi, X. P. Sun, Hydrothermal treatment of grass: a low-cost, green route to nitrogen-doped carbon-rich, photoluminescent polymer nanodots as an effective fluorescent sensing platform

- for label-free detection of Cu (II) ions. *Advanced materials*, 24 (2012) 2037-2041.
- [24] C. C. Huang, H. S. Li, C. H. Chen, Effect of surface acidic oxides of activated carbon on adsorption of ammonia, *Journal of Hazardous Materials*, 159 (2008) 523-527.
- [25] X. F. Jia, J. Li, E. K. Wang, One-pot green synthesis of optically pH-sensitive carbon dots with upconversion luminescence, *Nanoscale*, 4 (2010) 5572-5575.
- [26] C. Z. Zhu, J. F. Zhai, S. J. Dong, Bifunctional fluorescent carbon nanodots: green synthesis via soy milk and application as metal-free electrocatalysts for oxygen reduction, *Chemical Communication* 48 (2012) 9367-9369.
- [27] H. T. Li, Z. H. Kang, Y. Liu, S-T. Lee, Carbon Nanodots: Synthesis, Properties and Applications, *Journal of Materials Chemistry*, 22 (2012) 24230-24253.
- [28] P. Anilkumar, L. Cao, J. J. Yu, K. N. Tackett, P. Wang, M. J. Meziani, Y. P. Sun, Crosslinked carbon dots as ultra-bright fluorescence probes, *Small* 9 (2013) 545-551.
- [29] A. B. Bourlinos, A. Stassinopoulos, D. Anglos, R. Zboril, M. Karakassides, E. P. Giannelis, Surface functionalized carbogenic quantum dots. *Small* 4 (2008) 455-458.
- [30] S. Liu, J. Q. Tian, L. Wang, Y. W. Zhang, X. Y. Qin, Y. L. Luo, A. M. Asiri, A. O. Al-youbi, X. P. Sun, Hydrothermal treatment of grass: a low-cost, green route to nitrogen-doped carbon-rich, photoluminescent polymer nanodots as an effective fluorescent sensing platform for label-free detection of Cu (II) ions. *Advanced materials*, 24 (2012) 2037-2041.
- [31] S. N. Baker, G. A. Baker, Luminescent carbon nanodots: Emergent nanolights. *Angewandte Chemie International Edition*, 49 (2010) 6726-6744.
- [32] Q. H. Liang, W. J. Ma, Y. Shi, Z. Li, X. M. Yang, Easy synthesis of highly fluorescent carbon quantum dots from gelatin and their luminescent properties and applications, *Carbon* 46 (2013) 421-428.

- [33] Y M Guo, Z Wang, H W Shao, X Y Jiang, Hydrothermal synthesis of highly fluorescent carbon nanoparticles from sodium citrate and their use for the detection of mercury ions, *Carbon* 52 (2013) 583-589.
- [34] Q L Wang, H Z Zheng, Y J Long, L Y Zhang, M Gao, W J Bai, Microwave-hydrothermal synthesis of fluorescent carbon dots from graphite oxide, *Carbon*, 49, 2011, 3134-3140.
- [35] Fang Wang, Yonglai Zhang, Yang Liu, Xuefeng Wang, Mingrong Shen, Shuit-Tong Lee, and Zhenhui Kang, Opto-electronic conversion logic behavior through dynamic modulation of electron/energy transfer states at the TiO<sub>2</sub>-carbon quantum dot interface, *Nanoscale*, 2 (2013) 1831-1835.
- [36] S Nishimura, N Abrams, B A Lewis, L I Halaoui, T E Mallouk, K D Benkstein, J van de Lagemaat, A J Frank, Standing wave enhancement of red absorbance and photocurrent in dye-sensitized titanium dioxide photoelectrodes coupled to photonic crystals, *Journal of American Chemical Society* 125 (2003) 6306-6310.
- [37] Michele E. Lindesey, Michael Meyer, and E. M. Thurman, Analysis of Trace level of sulfonamide and tetracycline antimicrobials on groundwater and surface water using solid-phase extraction and liquid chromatography/mass spectrometry, *Anal. Chem.* 2001, 73, 4640-4646.